PII S1536-1632(02)00004-5

Molecular Imaging and Biology
Vol. 4, No. 3, 219–231. 2002

1536-1632/02 $–see front matter

Iterative Image Reconstruction for Clinical PET Using Ordered Subsets, Median Root Prior, and a Web-Based Interface

George Kontaxakis, PhD[1], Ludwig G. Strauss, MD[2],
Trias Thireou, MS[3], Maria J. Ledesma-Carbayo, MS[1],
Andrés Santos, PhD[1], Sotiris A. Pavlopoulos, PhD[3], Antonia Dimitrakopoulou-Strauss, MD[2]

[1]Technical University of Madrid (UPM), Department of Electronic Engineering, Madrid, Spain;
[2]German Cancer Research Center (DKFZ), Division of Oncological Diagnostics and Therapy, Heidelberg, Germany;
[3]National Technical University of Athens (NTUA), Biomedical Engineering Laboratory, Athens, Greece

Purpose: The development, implementation and validation of simple, flexible and efficient iterative image reconstruction (IIR) methods for their take-up in routine clinical positron emission tomography (PET) static or dynamic studies.
Procedures: The ordered subsets (OS) technique applied for the acceleration of the maximum likelihood expectation maximization (MLEM) IIR algorithm is here extended to include the weighted least-squares (WLS), image space reconstruction algorithm (ISRA) and the space alternating generalized EM (SAGE). The median root prior (MRP) has been successfully applied as a Bayesian regularization to control the noise level in the reconstructed images. All methods are implemented on distributed Pentium systems and tested using simulated PET data from a brain phantom. A Javascript is used for the initiation of the reconstruction.
Results: Taking into consideration the image quality and the time required for the reconstruction, the MRP-OSEM (ordered subsets expectation maximization) seems to provide best results after four to eight iterations, with four subsets and a MRP coefficient of 0.2–0.4. Iterative reconstruction of the transmission images with OS-acceleration and MRP regularization with subsequent calculation of the attenuation correction factors (ACFs) is shown to effectively remove streak artifacts in the emission images, especially along paths of high attenuation.
Conclusions: An efficient implementation using distributed processing principles and a web-based interface allows the reconstruction of one frame (with 63 cross-section slices) from a dynamic determination in few minutes. This work showed that regular PC systems can provide fast execution and produce results in clinically meaningful times. This eradicates the argument of the computational burden of the method that prevented the extensive use of IIR in today's modern PET systems. (Mol Imag Biol 2002;4:219–231)

Key Words: Iterative image reconstruction, Ordered subsets, Maximum likelihood expectation maximization, Median root prior, Attenuation correction factors, Distributed Pentium systems, Web-based interface.

Introduction

In emission tomography, images are obtained from a reconstruction process using a set of measured projections of the object or the patient examined. Iterative image reconstruction (IIR) methods have been lately proposed as alternatives to the conventional Fourier-based methods (traditionally used in X-ray computed tomography, CT). IIR techniques, despite their high computational cost, are becoming more and more popular, as they are shown to produce images of better contrast and signal-to-noise ratio than the conventional filtered back-projection (FBP).[1–3] The elimination of the streak artifacts[4] of the FBP with the use of iterative methods minimizes false-positive[5] as well as false-negative results, when lesions are situated in the vicinity of hot organs (such as the bladder). Furthermore, IIR algorithms have been shown to produce superior results than other conventional methods in other fields of imaging science and not only for the specific case of emission tomography.[6]

Until recently, the high computational cost and the dif-

Address correspondence to: George Kontaxakis, PhD, Universidad Politécnica de Madrid, Dpto. de Ingeniería Electrónica, E.T.S.I. de Telecomunicación, Ciudad Universitaria s/n, E-28040 Madrid. E-mail: g.kontaxakis@ieee.org

ficulty in controlling noise in the reconstructed images have not allowed the practical application of IIR in the clinical routine. Parallel implementations of the most popular IIR techniques have been proposed on dedicated architectures.[7–10] Although the computational efficiency has been significantly improved, the main disadvantages in the practical implementation of these approaches are their platform-dependency, high development and maintenance costs for their clinical use. The idea of distributed processing on a cluster of workstations becomes increasingly popular.[11] The main benefit of this approach is that a computationally intensive reconstruction task can be distributed on all the available computing capacity. In addition, local failures can be better tolerated in the context of distributed processing, as each reconstruction task is an independent process running on a system that depends only on the smooth functioning of the server and not on the rest of its clients.

Reconstruction task is the reconstruction of all studies (dynamic, multi-bed, multi-tracer) performed on all patients examined in one day. This task can be divided in subtasks, each of which refers to the iterative reconstruction of all time frames acquired at one bed position and with one tracer for one patient. Each subtask can be assigned to one of the available processors. The simultaneous use of several such processors that otherwise idle or carry out non-computationally intensive tasks, creates a quasi-parallel processing of all the available data to be reconstructed.

In this context, several IIR methods [maximum likelihood expectation maximization (MLEM[12,13]), weighted-least squares (WLS[14]), image space reconstruction algorithm (ISRA[15]) and space alternating generalized EM (SAGE[16])] are efficiently applied here for regular clinical use on distributed Pentium platforms, after initial testing on simulated brain phantom positron emission tomography (PET) data. The excellent computational capabilities of last-generation personal computing (PC) systems based on Pentium, or similar processors, and the large number of them usually available in a nuclear medicine department, make their use in carrying out tasks such as IIR quite appealing. The recently proposed ordered subsets (OS)[17] technique significantly accelerates the MLEM method [OSEM (ordered subsets expectation maximization) algorithm] and is here extended to the rest of the implemented IIR methods. These are also combined with a Bayesian technique[18] (median root prior, MRP) based on the one-step-late[19] approach, which employs a median filter regularization and efficiently removes noisy patterns, typical in images reconstructed with iterative algorithms based on probability methods after a large number of iterations,[1] without blurring the locally monotonic structures.[20]

Although the methods presented here are applied to two-dimensional (2D) sinograms, their application to three-dimensional (3D)-acquired PET data is straightforward. The most popular 3D protocols for IIR employ 2D rebinning of the 3D sinograms, using algorithms such as the Fourier Rebinning (FORE)[21] and then apply 2D algorithms to the rebinned sinograms. Therefore, reconstruction times for 3D PET data using FORE do not significantly differ from the ones reported here for 2D PET data, since the additional tasks of Fourier transform and rebinning do not require significant computational effort and time. Recently published results[22,23] have verified that application of FORE+OSEM does not show apparent image degradation compared with 3D-OSEM implementations.

Some manufacturers of PET scanners recently started to include in the software of their systems some IIR modules, mostly based on a simple version of the OSEM algorithm. The users, however, do not have the opportunity to easily change the various reconstruction parameters and optimize them to their acquisition protocols. Furthermore, they lack the flexibility to try different methods and easily change parameter sets in order to obtain valuable insight on the iterative techniques that become another black box for the average clinical user at the end. The danger in such cases is the application of iterative reconstruction for better images, but with the inappropriate parameter set and methods (commonly set during the installation of the PET scanner or the new software version and unchanged since then) the real outcome sometimes is bad images. In this paper, an integration of already existing IIR techniques is presented, implemented on a distributed network of common workstations, evaluated and validated on simulated and clinical PET data sets. The end-result of this work is a tool for the clinical physicians and scientists to easily understand, use and manage iterative image reconstruction in the daily routine of their nuclear medicine clinic.

The main focus of this manuscript is the presentation of an efficient and flexible implementation of IIR for PET, using distributed PC workstations, in an effort to bring IIR to the desktop of the physician and scientist at a PET Center with clinical orientation. All methods are carefully validated and evaluated using simulated PET data and then real clinical data sets. These investigations also provide significant results on the properties of the MRP and OS techniques in IIR and also reveal the importance of iterative attenuation correction for the accurate calculation of the attenuation coefficients for low-count emission studies.

The manuscript is organized as follows: In the following section are presented the methods implemented and their further development in the framework of this project, along with the major figures of merit used for the evaluation and validation of these techniques. A separate section is dedicated to their implementation on distributed platforms, entering in some detail in order to give a clear description of each step and allow the immediate take-up and application of the techniques presented in the clinical routine of an average PET unit.

The methods used for the calculation, storage and retrieval of the transition matrix are also presented in detail, as they represent the key for the fast and efficient implementation of IIR. The Results section first presents a validation of the methods developed and implemented with the use of simulated PET data from the Hoffman Brain Phantom, in order to justify their application on real PET patient data. The clinical evaluation includes an investigation on the selection of the best set of parameters for the IIR of data obtained by a typical PET acquisition protocol from the PET Center participating to this work. The time performance of the implementation of the presented techniques is given in the same section, together with the discussion of the major findings that are also summarized in the Conclusions section.

Methods

Iterative image reconstruction methods with Bayesian prior typically update the value of voxel i in the image vector $\mathbf{x}$ at the k^{th} iteration according to the following multiplication scheme:

$$x_i^{(k)} = M_i^{(k-1)} \cdot C_i^{(k-1)} \cdot x_i^{(k-1)},\ i = 1,2,...,I \qquad (1)$$

where I is the total number of voxels and $\mathbf{M}^{(k)}$ and $\mathbf{C}^{(k)}$ are the vectors of the regularization prior (here MRP) and voxel-update coefficients respectively at the k^{th} iteration. The elements of the vector of MRP coefficients are calculated according to the following scheme:

$$M_i^{(k)} = \left(1 + \beta \frac{x_i^{(k)} - med(x_i^{(k)}, i)}{med(x_i^{(k)}, i)}\right)^{-1} \qquad (2)$$

where $med(\mathbf{x},i)$ is the median over a neighborhood of the voxel i. In the implementation presented here a 3×3 median filter is used. The term β represents the prior weight and ranges from 0.0 to 1.0.

The updating coefficients $\mathbf{C}^{(k)}$ are calculated using the vector $\mathbf{y}$ of the measured sinogram data and the forward-projection of the estimated image vector $\mathbf{x}^{(k)}$ to the data space, using a projector operator $\mathbf{P}$ and vice-versa (from the data space to the image space) with its transpose $\mathbf{P}^{\mathbf{T}}$. The MLEM, SAGE, WLS, and ISRA techniques employ different schemes involving the projection-backprojection operator $\mathbf{P}$ to compute the correction coefficients, as shown in the following equations :

$$\text{MLEM: } \mathbf{C}^{(k)} = \mathbf{P}^{\mathbf{T}}[\mathbf{y}/\mathbf{P}[\mathbf{x}^{(k)}]] \qquad (3)$$

$$\text{SAGE: } \mathbf{C}^{(k)} = \mathbf{P}^{\mathbf{T}}[\mathbf{y}/\mathbf{P}[\mathbf{x}^{(k)}]] \qquad (4)$$

where $\mathbf{P}[\mathbf{x}^{(k)}]$ is continuously updated

$$\text{WLS: } \mathbf{C}^{(k)} = \mathbf{P}^{\mathbf{T}}[(\mathbf{y}/\mathbf{P}[\mathbf{x}^{(k)}])^2] \qquad (5)$$

$$\text{ISRA: } \mathbf{C}^{(k)} = \mathbf{P}^{\mathbf{T}}[\mathbf{y}]/\mathbf{P}^{\mathbf{T}}[\mathbf{P}[\mathbf{x}^{(k)}]] \qquad (6)$$

Applications of iterative techniques based on probability methods for image restoration and reconstruction have been reported since the early 1970s, both in general framework,[24] as well as for specific applications, like astronomy.[25] Later, the maximum likelihood (ML) approach for image reconstruction in emission tomography was introduced by Rockmore and Macovski in 1976.[26] This was followed by the presentation of the general mathematical statistics framework of the expectation-maximization (EM) algorithm by Dempster et. al in 1977.[27] A practical implementation of the MLEM algorithm to the problem of image reconstruction in PET has been presented by Shepp and Vardi in 1982[12] and extended to the transmission case by Lange and Carson in 1984.[13]

The MLEM algorithm provides an iterative formula to solve the problem of image reconstruction in emission tomography. It maximizes the probability (likelihood) of observing the given counts in the coincidence detector tubes if the true activity distribution in the source is $\mathbf{x}$, under a Poisson probability model for the positron emissions. This probability is expressed in the formulation of the projector operator $\mathbf{P}$ as a transition law between the data and the image space. It is described by the elements $a(i,j)$ of the transition matrix, as the probability for an annihilation event in the area covered by voxel i to be registered in the line-of-response (LOR) j.

The SAGE algorithm[16] uses the forward projection of the image estimate to calculate the correction factors (according to the MLEM scheme) for the update of one or a selected subgroup of image voxels during one iteration. The ISRA has been proposed[15] in order to reconstruct data from a tomograph with a spatially variant point spread function. The ISRA was later found[28] to converge to a non-negative solution of the least-squares estimator of the emission densities, provided that a strictly positive starting point is used. The WLS algorithm has been recently proposed[14] in order to improve the convergence rate of IIR compared to the MLEM algorithm. Other formulations for iterative image reconstruction based on weighted least-squares exist,[29,30] but in this paper the WLS algorithm refers exclusively to the formulation expressed in Equation 5. To the knowledge of the authors, however, none of these three algorithms has been applied to clinical PET data, apart from the research publications referring to these methods.

Slow convergence rate is one of the major drawbacks of IIR algorithms, like the MLEM. This means that it takes several iterations to reach the maximum, or at least a near-maximum value, of the objective function (likelihood).[31] Another problem associated with this issue is the lack of a robust stopping rule that can dictate the termination of the iterative process, although some attempts have been made in the past towards this direction.[32–34] This is mainly due to the fact that direct implementation of the MLEM algorithm or other similar ones is inherently unstable and statistical noise is added

to the reconstructed images as the iterations proceed.[1] To remedy this situation, Bayesian approaches,[35] such as the MRP method used here, have been proposed as an alternative to the early stopping of the iterative process and possible post-reconstruction filtering and smoothing of the images.

Transmission scans are usually associated with emission tomography studies, as they are used to obtain an estimation of the attenuation properties of the body under investigation. Iterative reconstruction of the transmission images also shows significant improvement in image quality and accuracy of the estimation of the attenuation correction factors (ACF) in comparison with the conventional FBP methods applied in other transmission tomography modalities. The emission sinograms are then multiplied pixel-by-pixel with the ACF values calculated based on a pair of transmission scans, with and without the patient on the bed of the tomograph, and with the use of the external radioactivity sources mounted on the scanner for this purpose.

The iterative gradient algorithm (GA)[36] for the reconstruction of the transmission images has been used here. This is mainly because of the simplicity in its formulation and implementation and its reported satisfactory performance.[37] The MRP method can be also applied for the case of transmission image reconstruction. If μ is the attenuation parameter vector, its update at the k^{th} iteration according to the MRP-GA is given by:

$$\mu_i^{(k)} = M_i^{(k-1)} \cdot C_i^{(k-1)} \cdot \mu_i^{(k-1)} \tag{7}$$

where the MRP vector $\mathbf{M}^{(k)}$ is calculated as described in Equation 2, by replacing the image vector $\mathbf{x}^{(k)}$ with the vector of the attenuation parameters $\boldsymbol{\mu}^{(k)}$. The updating coefficient $\mathbf{C}^{(k)}$ for the case of GA is given by:

$$\mathbf{C}^{(k)} = \mathbf{P}^{\mathbf{T}}[\tilde{\mathbf{y}}^{(k)}_{\mathbf{T}}] / \mathbf{P}^{\mathbf{T}}[\mathbf{y}_{\mathbf{T}}], \quad \text{where } \tilde{\mathbf{y}}^{(k)}_{\mathbf{T}} = \mathbf{y}_{\mathbf{B}} \cdot e^{-\mathbf{P}[\mu^{(k)}]} \tag{8}$$

In the above equation $\mathbf{y_T}$ and $\mathbf{y_B}$ are the transmission and blank scan sinogram data vectors respectively. If the attenuation parameters are known, the ACFs can be computed from the expression $e^{\mathbf{P}[\mu]}$, whereas the conventional method employs the smoothed ratio $\mathbf{y_B} / \mathbf{y_T}$. The implementation described in the next section provides the user with the option to select either the conventional method for attenuation correction or the correction of the emission data after iterative transmission image reconstruction.

Ordered subsets acceleration of the MLEM reduces the number of iterations needed by a factor equal to the number of subsets used, while maintaining the image quality when the number of subsets is not too high. This has been initially shown by Hudson and Larkin in 1994[17] and later verified by various experiments by other scientists,[38] thus working towards the application of IIR in clinically meaningful times. The OS technique has been widely adopted by the imaging community and an extensive literature already exists on this kind of block-iterative reconstruction methods,[39] permitting a detailed knowledge of the statistical properties of such methods, the proper subset selection,[40] etc. As in the case of the application of the OS technique in emission tomography, it has been shown that the same approach speeds up the increase in the objective function by roughly the number of subsets in the early iterates when compared to the ordinary transmission image reconstruction algorithms.[41] Recent work[42] has also demonstrated the efficiency of the MRP technique in improving image quality for low-count transmission images reconstructed with the OSEM algorithm for the transmission case. Parallel implementations of the OSEM method on distributed processors have been also presented.[43] The OS technique is here extended to the other IIR methods and, in combination with the Bayesian prior, the new algorithms MRP-OSWLS (ordered subsets weighted least-squares), MRP-OSISRA (ordered subsets image space reconstruction algorithm), MRP-OSSAGE (ordered subsets space alternating generalized expectation maximization), as well as the MRP-OSGA (ordered subsets gradient algorithm) for the transmission case are developed, implemented and evaluated on static and dynamic PET determinations.

An ECAT EXACT HR+ (CTI/Siemens, Knoxville, TN) tomograph was used for the patient studies. A model of this camera is created and its basic configuration is used in order to calculate the values of the transition matrix. The tomograph delivers images in 63 planes (32 direct and 31 cross-planes) and has an axial field-of-view (FOV) of 15.5 cm. It is constructed using four rings of 72 8 × 8 BGO detector blocks. Each of its 32 rings consists of 576 individual detector crystals, each of dimensions 4.39 × 4.05 × 30 mm^3 and images a transaxial FOV of 56.2 cm. A typical dynamic study is composed of 23 frames acquired for 60 minutes, immediately following intravenous injection of 2-deoxy-2-[^{18}F]fluoro-D-glucose (FDG): 10 frames of 60 seconds, five frames of 120 seconds and eight frames of 300 seconds. A total of 1449 slices are reconstructed from the dynamic series. Besides the dynamic acquisition, additional static emission scans are performed for up to three different bed positions around the main position of the dynamic measurement. All emission acquisitions are preceded by transmission scans (10-minute dynamic scan, 5-minute post-injection for the static scans) for the attenuation correction.

The figures of merit (FOM) used in the comparative studies of the reconstructed images are the noise, the contrast, the signal-to-noise ratio (SNR) and the reconstruction time. The noise is calculated as the ratio σ_R / μ_R, where σ_R and μ_R are the S.D. and the mean of the values of 500 randomly selected pixels in a region-of-interest (ROI). The contrast is measured as: $CR=(R-B)/B$, where R and B are the summed activities of 500 randomly

selected pixels of a region and its background respectively. The SNR is calculated as: $SNR = CR / (\sigma_B / \mu_B)$.

The IIR methods implemented, including the application of Bayesian priors, produce non-negative images (no voxels contain negative values), but not all of them show the self-normalization property, characteristic of the MLEM algorithm. Therefore, a normalization step is performed at the end of each reconstruction task in order to obtain quantitative images. Since the current implementation represents a direct clinical application, the standard uptake values (SUVs) displayed are therefore independent of the reconstruction method selected and only depend on the inherent noise and convergence characteristics of the IIR method applied for each case. A detailed study on the effects of the reconstruction parameters of the same methods presented here on the SUVs for clinical cases has been recently presented by Strauss et al.[44]

Implementation

The Concept of "Quasi-Parallel" Processing

The implementation is performed using C/C++ on Pentium (Intel Corp., Santa Clara, CA) systems under Windows NT[45] (Microsoft Corp., Redmond, WA). After acquisition all patient data are transferred from the console of the tomograph to a Windows NT 4.0 PC server using file transfer protocol (FTP). IIR reconstruction and further analysis of the collected sinograms are carried out on a separate local network of PCs,[44] typically available on the desktops of the members of a PET group in a clinic. In this way, the tomograph's console and its client workstations are not loaded with reconstruction and other post-processing tasks.

The IIR software is manually started as an independent process on any available workstation (client) with access to the patient database on the NT server. All clients are connected to the NT server using TCP/IP. Most of the clients used for the experiments described here run Windows (95/98/NT4.0/2000) operating systems. Successful tests, however, have been carried out using BeOS V4.5 (Be Inc., Menlo Park, CA) and Linux SuSE 6.2 (SuSE GmbH, Nürnberg, Germany). All data given in the Results section regarding the performance of the iterative reconstruction schemes are carried out on Windows NT 4.0 workstations.

Instead of asking on-line for data, each process regularly checks a dedicated queue on the server for a reconstruction task (or subtask, as explained in the previous section). The user introduces a reconstruction task for a desired patient study to this queue using a Web-based interface. This can be accessed through the Internet at: http://www.dkfz.de/pet/itmail5.htm. This allows the user to submit a reconstruction request at any time and from any workstation with access to Internet, without direct interaction with the running code. When the Web form is completed and submitted, the parameters selected are transferred to the queue on the reconstruction server via SMTP (as an e-mail message) and stored as new tasks. To avoid execution of unauthorized requests, the server recognizes only reconstruction requests sent by authorized users. When a new valid request arrives, the next available workstation undertakes the task. In case no workstation is available upon the arrival of the request to the reconstruction queue, this request is stored first-in first-out at that queue. A quasi-parallel scheme is hence achieved, since several requests can be executed at the same time, as many as the number of different instances of the IIR software that are active at that moment on the operating workstations available on the subnet.

Except for the launch and termination of the reconstruction software on each workstation and the submission of the reconstruction parameters via the Web interface, all other processing is carried out automatically and does not require the interaction of a user at any moment. During the performance of a specific reconstruction task, all calculations and temporary data storage are done on the executing client workstation. Upon successful completion of each requested task, the image data are stored back to the database with the patient data and all temporary data files deleted from the client. In case the reconstruction is not successfully completed, a message is issued and stored at a separate dedicated queue on the reconstruction server. The administrator can then rectify the problem and re-submit the request.

The use of distributed PCs in network within (or even outside) the medical PET clinic makes optimal use of the computing power of these systems that remains unused while these either idle or are dedicated to simple secretarial or basic communication (e-mail, Internet access, etc.) tasks. In addition, the transfer of image reconstruction tasks to PCs removes the corresponding workload from the tomograph's console and associated workstation network (typically limited to one to two Unix-based workstations). As a result, this minimizes potential problems during the crucial phase of data acquisition and allows better allocation of their computing capabilities to tasks such as research and development activities.

The Transition Matrix

A major problem for an efficient implementation of IIR methods using a projector operator **P** is the size of the transition matrix. Since this is highly sparse, its non-zero elements are pre-computed using a Monte Carlo technique,[45] based exclusively on the geometric model of the tomograph's design and its field of view, and loaded during the reconstruction using an efficient sparse-matrix technique. All non-zero elements of the matrix are stored in a static array. A lookup table keeps a counter of the non-zero values for each pixel and eliminates the need to

store the *i*- (voxel) coordinate for each element. The *j*- (LOR) coordinate, however, is still needed since for each voxel a different set of LORs contributes to its non-zero elements in the matrix. A 16-bit unsigned integer stores the *j*-coordinate for each element. The value of the probability *a(i,j)*, typically ranging from .0001 to .001 for a 256 × 256 image grid size, can be encoded in a 16-bit unsigned integer if multiplied by a factor of 10^6 and truncated. In addition, very small values of the *a(i,j)* can be considered as zero, without significant degradation of the quality of the reconstructed images. Therefore, a significant amount of memory and execution time is saved.

For ordered-subsets implementations with non-overlapping subsets, all non-zero elements related to one subset are sequentially stored in memory, followed by the elements related to the next subset. If $N_{i,s}$ is the number of non-zero elements for voxel i for subset s (stored in a look-up table), the structure of the memory where the matrix is loaded for s non-overlapping subsets, is shown in Figure 1).

All algorithms described above can be efficiently implemented using the above matrix representation. For OS-implementations using non-overlapping subsets, one cycle is performed for each subset using the appropriate memory segment that contains the portion of the transition matrix corresponding to the current subset.

The exclusive use of the geometrical characteristics of the system in the calculation of the probability matrix *a(i,j)* could lead to a significant reduction in the number of the non-zero elements of the matrix that need to be stored, if the symmetry of a detector ring and an image grid centered in it are considered.[10] In this work, however, the symmetry of the tomograph model was not used in order to present an implementation that could be easily expanded and applied to systems without circular symmetry or when other parameters are included in the calculation of *a(i,j)*. In addition, the unfolding of the matrix in that case also increases the computational effort with the necessary decoding calculations.

Direct zooming in the FOV during reconstruction is also possible using a coarser grid for the area in the FOV outside the visible image grid. Iterative reconstruction using transition matrix requires that reconstruction be carried out over the whole FOV. In this way, all measured sinogram counts are distributed to the voxels. The use of a transition matrix, however, does not require the same size or shape for all voxels. The area between the tomograph's FOV and the visible image grid boundary is divided in successive square frames (typically 20) of increasing size and considered as individual voxels.[46] Currently, supported zoom factors are 1.5 and 2.0. Alternatively, one can always request a reconstruction for the entire FOV and interpolate the reconstructed slices to the desired zoom.

Results

Results from Phantom Simulations

In order to evaluate the performance of the algorithms developed before applying them on real clinical cases, a series of phantom simulation investigations have been carried out. As a source, one slice of a 3D brain phantom has been used. This phantom, also known as Hoffman Brain Phantom,[47] simulates the activity distributions found in the human brain for the case of PET. It was initially developed from a series of magnetic resonance imaging (MRI) scans taken at 7 mm intervals over a whole brain. These images have been digitized and segmented in two main activity areas representing the gray and white matters. These are shown as two layers, with gray to white ratios of 5 to 1. A third area with zero activity corresponds to the ventricles and the background space.

For this study, slice 14 (there is a total of 18 slices in the Hoffman Brain Phantom) has been selected as virtual activity distribution within the FOV of one ring of the ECAT EXACT HR+ tomograph (Figure 2A). A Monte Carlo routine has been developed for the generation of Poisson distributed annihilation events under ideal conditions (no attenuation, scatter or random coincidences) in the active areas of the phantom, according to the physics of positron emission. Each event

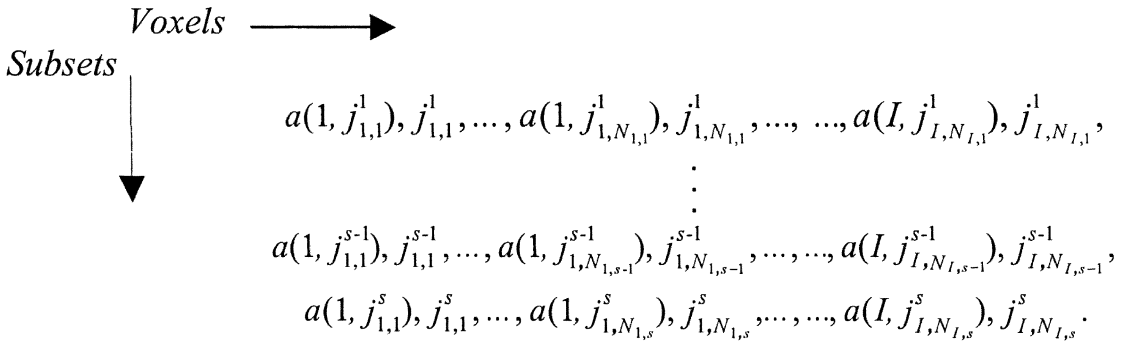

Figure 1. The structure of the memory where the matrix is loaded for **s** non-overlapping subsets.

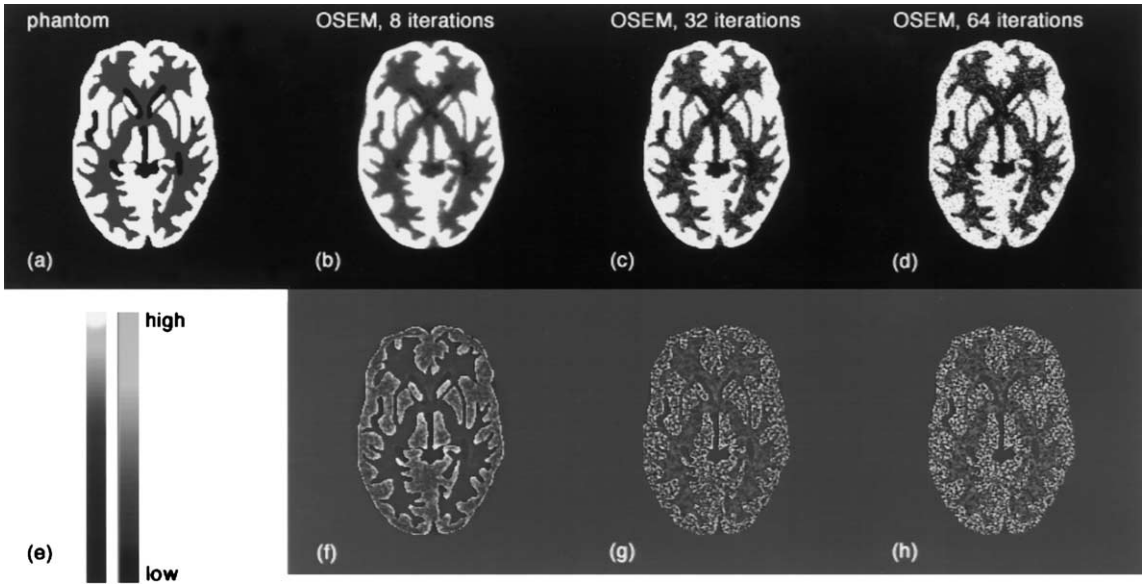

Figure 2. All images are of size 256 × 256. (A) Phantom image (slice 14 of the Hoffman Brain Phantom); (B)–(D) reconstructed images from noise-free sinogram data generated from the phantom activity distribution, using the OSEM method, four subsets and no MRP, after eight, 32, and 64 iterations; (E) the color scales used for the display in Figures 2–4 (right bar for upper row, left bar for lower row); (F)–(H) quantitative subtractions (difference images) of the reconstructed images shown in (B)–(D) from the phantom activity distribution. Each of the groups (B)–(D) and (F)–(H) are displayed with the same window/level thresholds, in order to be visually comparable.

produces a pair of γ-rays that travel in exactly opposite directions, which are assumed to be detected by the scintillation detectors and correctly identified. At the end of each data-generation experiment, the collected counts are sorted into a sinogram of the same format used by the ECAT software, ready for reconstruction. These data are adequate for the initial evaluation of the IIR methods implemented.

Figure 2 shows iteratively reconstructed images with the OSEM method (four subsets) without MRP and for 8, 32, and 64 iterations (results equivalent to 32, 128, and 256 iterations of the MLEM method, Figure 2B–D), from noise-

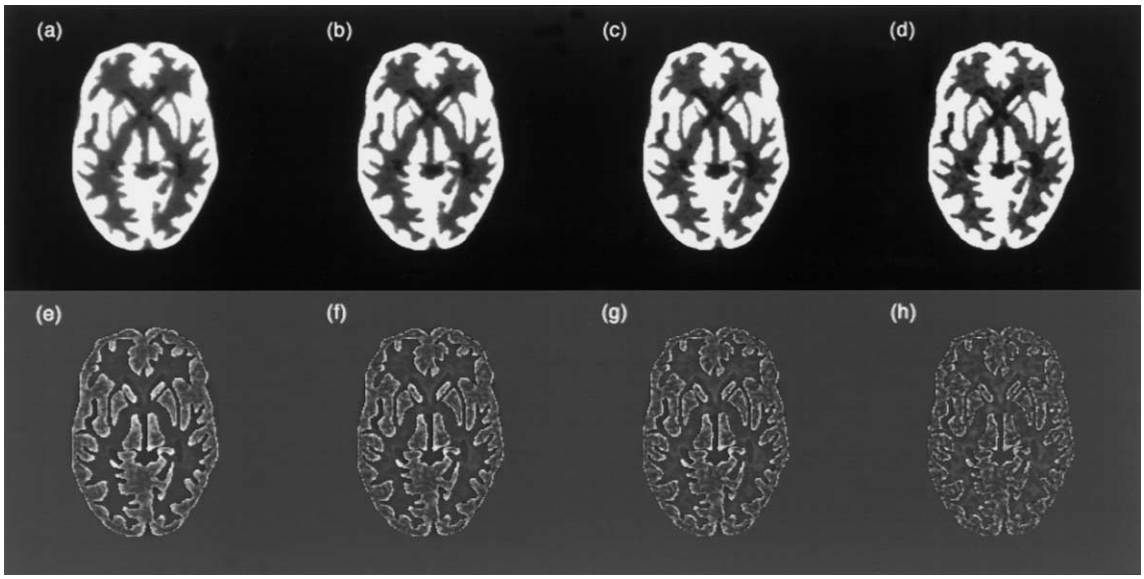

Figure 3. All images are of size 256 × 256. Reconstructed images from noise-free sinogram data generated from the phantom activity distribution (Figure 2A), with the OSEM method, four subsets, MRP with $\beta = 0.2$ and (A) eight iterations, (B) 12 iterations, (C) 16 iterations, and (D) 32 iterations. (E)–(H) Quantitative subtractions of the reconstructed images shown in (A)–(D) from the phantom activity distribution. Each of the groups (A)–(D) and (E)–(H) are displayed with the same window/level thresholds, in order to be visually comparable.

free PET data (6,079,000 counts) generated with the method described above. The characteristic speckled noise added to the reconstructed images as the iterations proceed is clearly visible, especially to the results after 32 and 64 OSEM iterations. The quantitative subtractions (difference images, Figure 2F–H) of these results from the initial activity distribution (Figure 2A) are also shown and clearly depict the noise level introduced to the reconstructed images, when the iterative procedure is carried out for an excessive number of iterations.

The application of the MRP method aims to the efficient control of the added noise without affecting the image quality and its quantification characteristics. Figure 3 shows images from the same data set as the ones shown in Figure 2, after 8, 12, 16, and 32 iteration steps of the OSEM algorithm (four subsets) with the use of the MRP with $\beta = 0.2$. The results show that the noise has been efficiently removed from the reconstructed images (compare Figure 2C with Figure 3D) whereas edge information is kept intact. The corresponding difference images (Figure 3E–H) of these results from the phantom image verify the elimination of noise. The error is still larger at sharp edges, diminishing as the number of iterations increases.

The other IIR methods examined here produce similar results, both visually and quantitatively. Figure 4 shows images reconstructed from the same data set and with the same parameters as Figure 3C, using OSISRA (Figure 4A), OSSAGE (Figure 4B), and OSWLS (Figure 4C). Even though the visual comparison of the reconstructed images does not reveal marking differences between them, the quantitative subtraction of the results shown in Figure 4 from the OSEM reconstructed image (Figure 4D–F) clearly shows the underlying differences in the convergence of each method. OSISRA shows characteristic streak lines, due to the nature of the algorithm. This updates the image vector based on ratios of backprojections (Equation 6). OSSAGE does not significantly differ from OSEM, whereas OSWLS shows slight difference in noise (higher noise levels in high-activity areas) characteristics. These differences, however, are visible only within a narrow window/level threshold. Quantitative subtraction of the OSISRA, OSAGE, and OSWLS images from the phantom image verify the visual resemblance of these results with the ones obtain with the OSEM method (Figure 4G–I), where differences are stronger near sharp edges.

Results from Clinical Application

The iterative image reconstruction methods have been then applied to real clinical data from a PET dynamic FDG liver metastasis study. Tables 1 and 2 show the reconstruction times for image sizes 128×128 and 256×256 on a Pentium II (450 MHz, 256 MB RAM). Reconstruction times are shown in seconds without MRP for one slice and with 1, 4, 8, or 16 subsets while keeping

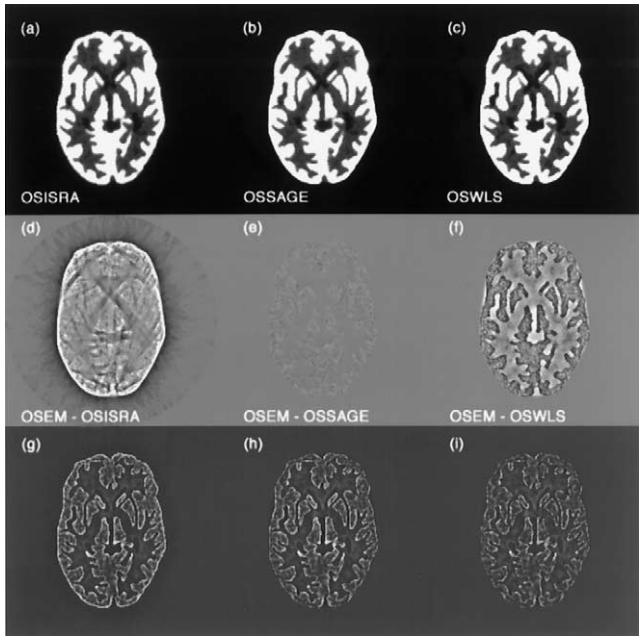

Figure 4. All images are of size 256×256. Reconstructed images from noise-free sinogram data generated from the phantom activity distribution (Figure 2A), after 16 iterations with four subsets, MRP with $\beta = 0.2$ and the (A) OSISRA, (B) OSSAGE, and (C) OSWLS methods. (D)–(F) Quantitative subtractions of the reconstructed images shown in (A)–(C) from the image reconstructed with the same parameters using the OSEM method (Figure 3C). (G)–(I) Quantitative subtractions of the reconstructed images shown in (A)–(C) from the phantom activity distribution. Each of the groups (A)–(C), (D)–(F), and (G)–(I) are displayed with the same window/level thresholds in order to be visually comparable.

constant the product: *(number of iterations)* $\times$ *(number of subsets)* $= 64$. The execution time for one iteration (over all subsets) is given in subscript. These results show that one to two seconds are required per iteration and one complete plane (in this case from a static sinogram that resulted from the addition of the six last frames of the dynamic study) can be reconstructed within 0.5–1.0 minute (depending the image size and the method selected). This makes possible the iterative reconstruction of a complete sinogram from the tomo-

Table 1. Reconstruction times (seconds) for one slice of size 128×128 (in subscript for one iteration over all subsets) on a Pentium II (Windows NT 4.0) at 450 MHz for image quality equivalent to 64 iterations of MLEM

	Subsets–Iterations			
Methods	**1–64**	**4–16**	**8–8**	**16–4**
OSEM	$27.4_{0.4}$	$7.5_{0.5}$	$4.0_{0.5}$	$2.2_{0.6}$
OSISRA	$26.9_{0.4}$	$7.8_{0.5}$	$4.2_{0.5}$	$2.3_{0.6}$
OSWLS	$27.4_{0.4}$	$7.5_{0.5}$	$4.0_{0.5}$	$2.3_{0.6}$
OSSAGE	$49.4_{0.8}$	$12.9_{0.8}$	$6.7_{0.8}$	$3.6_{0.9}$

Table 2. Reconstruction times (sec) for one slice of size 256 × 256 (in subscript for one iteration over all subsets) on a Pentium II (Windows NT 4.0) at 450 MHz for image quality equivalent to 64 iterations of MLEM

	Subsets–Iterations			
Methods	**1–64**	**4–16**	**8–8**	**16–4**
OSEM	$96.9_{1.5}$	$26.3_{1.6}$	$14.0_{1.8}$	$7.9_{2.0}$
OSISRA	$96.4_{1.5}$	$27.8_{1.7}$	$14.9_{1.9}$	$8.5_{2.1}$
OSWLS	$96.8_{1.5}$	$26.2_{1.6}$	$14.1_{1.8}$	$8.0_{2.0}$
OSSAGE	$176.3_{2.8}$	$46.1_{2.9}$	$24.0_{3.0}$	$13.3_{3.3}$

graph used in less than 35–45 minutes. Shorter reconstruction times have been demonstrated, as expected, with the use of faster Pentium platforms.[44] Trials of the same methods under different operating systems (Linux and BeOS) showed lower reconstruction speeds, possibly due to the use of standard compilers of these operating systems, without particular optimization schemes on the compiled C code.

The efficiency of the implementation can be shown by comparing similar results published in recent literature and with the use of similar PC equipment, where 0.85 s/iteration for the OSEM method are reported by Toft[48] on image size 101 × 101, whereas here 0.4 s/iteration are obtained for a larger image size of 128 × 128, but also a somehow faster computing platform. All measurements reported here are performed on PC systems under Windows NT 4.0.

The OSEM, OSWLS, and OSISRA show similar performance in execution times, whereas the OSSAGE requires about twice the time for the same number of iterations, as it required the reprojection of the image vector to the data space after each pixel update during one iteration. More recent modifications of the SAGE algorithm (SAGE–3)[49] might provide better acceleration factors and image quality. The application of the MRP penalty after each iteration increases the reported times by 10–15%.

For the selection of the most appropriate parameters set (number of subsets and iterations and value of the MRP coefficient β), the reconstructed images have been quantitatively studied as a function of these factors on the same sample of clinical patient data from a dynamic (23 frames) FDG-PET determination of a liver metastasis. This has been a typical study (in terms of measured counts, shape of imaged organ and image reconstruction protocol) in the clinical routine at DKFZ. The last six frames (18 to 23) are summed up and slices 20 to 30 are reconstructed. In each study, two of the three parameters are kept constant while the third one varies. The constant values are four iterations, six subsets, and $\beta = 0.3$.

When the number of iterations varies from two to 10, the quality of the reconstructed images shows the typical deterioration with increasing number of iterations for the OSSAGE, OSEM, and OSWLS methods, while the OSISRA images keep improving up to 10 iterations, but with subsequent increase in the reconstruction time. The OSISRA shows, however, increased streak artifacts, and blurs the body and ROI contours. Table 3 summarizes these results and the MRP-OSEM and MRP-OSSAGE algorithms seem to be the methods of choice when (*iterations* × *subsets*) reaches the values around 24–30, with the latter, however, being more computationally intensive than the former, as shown above.

A similar determination using four and eight subsets showed that an increasing number of subsets results in a slightly lower image quality. This is expected, since the number (4) of iterations is kept constant therefore the quality of the resulting images with four subsets corresponds to the result of 16 iterations without subsets. With eight subsets the results are equivalent (in the sense that one can consider equivalent the resulting images from different reconstruction experiments where the product (*iterations* × *subsets*) is constant[17]) to the ones obtained after 32 iterations without subsets. Table 4 summarizes the results of this work. Once again, the OSEM algorithm provides the best result.

The selection of the parameter β largely depends on the specific algorithm used. Table 5 summarizes the results of an investigation performed by keeping the number of iterations and subsets constant and varying β from 0.1 to 0.9. The OSSAGE algorithm provides the best results with $\beta = 0.3$, but requires the longest reconstruction time, whereas the OSEM algorithm provides similar results with $\beta = 0.4$ and requires the shortest reconstruction time. In the literature, there is relatively little reference to investigations for the proper selection of this parameter. Seret[50] evaluated the MRP-OSEM method for SPECT image reconstruction and concluded that the Bayesian coefficient should not exceed 0.3 in order to avoid loss or

Table 3. Image quality variations with the number of iterations (for six subsets with $\beta = 0.3$)

	Best Value			Worst Value		
Method	**Iterations**	**Contrast**	**SNR**	**Iterations**	**Contrast**	**SNR**
OSSAGE	4	1.172	0.940	10	0.916	0.708
OSEM	4	1.132	0.904	10	0.704	0.620
OSWLS	4	0.995	0.798	10	0.764	0.570
OSISRA	10	0.864	0.642	2	0.178	0.163

Table 4. Image quality variations with the number of subsets (over four iterations with $\beta = 0.3$)

	Best Value			Worst Value		
Method	**Subsets**	**Contrast**	**SNR**	**Subsets**	**Contrast**	**SNR**
OSSAGE	4	1.042	0.849	8	0.950	0.724
OSEM	4	1.067	0.862	8	0.893	0.681
OSWLS	4	0.971	0.798	8	0.760	0.568
OSISRA	4	0.320	0.288	8	0.540	0.445

resolution in the reconstructed images. Liow and Zhou[51] arrive to a similar conclusion after a detailed study of this Bayesian parameter, among others, on 3D PET data and with different iterative reconstruction methods. The size of the median filter is also of importance and is here maintained to the minimum size of 3×3. This is done in order to avoid excessive blurring of the reconstructed images, as well as to keep low the computational overload. To further improve the quality and appearance of the reconstructed images with MRP, Alenius and Ruotsalainen[52] recently proposed the use of a generalized class of MRP-type of priors, with the replacement the standard median by other order statistics operations. These methods capture sharp changes in piece-wise constant signals and preserve signal features, while eliminating time high frequency noise. These techniques have not been implemented in the present work, as their application introduces further parameters and optimization investigations that complicate the practical implementation of the methods presented without significant contribution to image quality improvement for the routine clinical use.

Based on the results of the above study, in the clinical routine at the Medical PET Group of the German Cancer Research Center, the MRP-OSEM reconstruction method is used for the patient data, using four subsets and four to eight iterations. The standard low-count dynamic emission acquisition protocols employed do not allow the use of more subsets and the above-mentioned quantitative study on a representative sample of patient data verified that four is the optimal number of subsets for this kind of data. Values of 0.2–0.4 for the MRP coefficient are currently used, as higher values might excessively blur the reconstructed images and reduce contrast and small lesion detectability. With the implementation scheme described earlier, it takes about three to four hours for the reconstruction of a complete dynamic study (23 frames of 63 slices each) using MRP-OSEM on a PC under Windows NT 4.0. For a typical whole-body investigation with five bed positions, results can be obtained in less than one hour, with the first images obtained even before the patient leaves the tomograph's bed.

Table 5. Image quality variations by changing the MRP coefficient (over four iterations and six subsets)

	Best Value			Worst Value		
Method	**β**	**Contrast**	**SNR**	**β**	**Contrast**	**SNR**
OSSAGE	0.3	1.118	0.906	0.9	0.999	0.817
OSEM	0.4	1.087	0.883	0.1	0.982	0.786
OSWLS	0.6	0.954	0.658	0.9	0.819	0.557
OSISRA	0.8	0.530	0.457	0.1	0.431	0.369

Figure 5 shows one cross section from a dynamic liver study with FDG, showing a large metastatic lesion on the left liver lobe, iteratively reconstructed using the methods presented here. The last time frames (12 to 15) have been added together and reconstructed using four subsets and six iterations and a $\beta = 0.2$ of the MRP coefficient. The MRP-OSISRA technique shows increased streak artifacts, and blurs the body and ROI contours. The MRP-OSSAGE is not providing any visible improvement from the MRP-OSEM. The difference images in Figure 6 verify these observations (quantitative difference of the MRP-OSISRA, MRP-OSSAGE, and MRP-OSWLS images from the one reconstructed with MRP-OSEM).

A characteristic streak artifact along the arms is visible

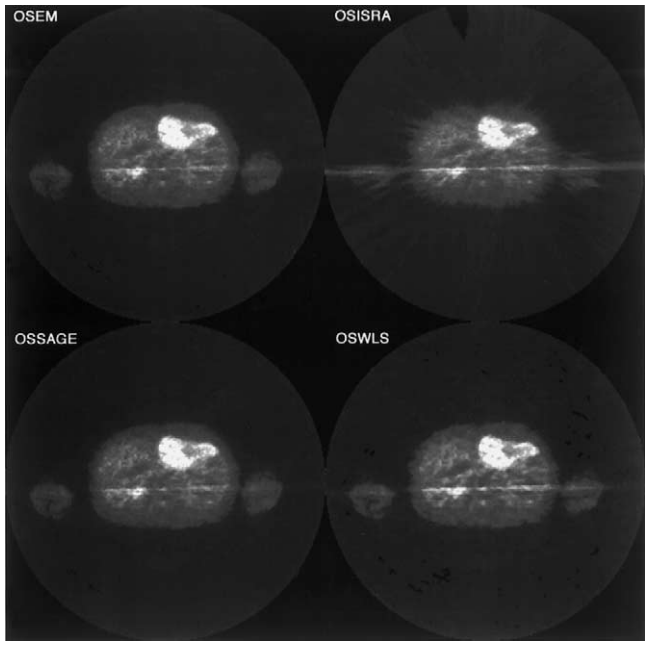

Figure 5. Cross sections from a liver study (metastatic lesion on the left lobe) with FDG reconstructed with OSEM (upper left), OSISRA (upper right), OSSAGE (lower left), and OSWLS (lower right), with MRP ($\beta = 0.2$), four subsets and six iterations.

in all images due to the limited attenuation correction scheme applied to the measured data. The inefficient attenuation correction is mainly due to the fact that the transmission scans, particularly on long attenuation paths such as horizontal lines along the arms, contain very few events in several projections. This problem is accentuated after randoms correction since several of these LORs contain relatively large negative values that render the calculation of the ACFs even more imprecise. Therefore, measured attenuation correction using calculated ACFs from the ratio of a smoothed blank and a transmission scan is not adequate for short-interval 2D dynamic acquisitions with a low-count short transmission scan. Alternatively, the ACFs can be computed by using a forward projection of the attenuation μ-maps generated by iterative reconstruction of the transmission scans.

Attenuation correction with ACFs calculated with the measured attenuation correction of the tomograph's software produces an image with strong streak artifacts that can potentially lead to false-positive diagnoses. Figure 7 shows the same cross section displayed in Figure 5, iteratively reconstructed using the same reconstruction parameters with OSEM and OSISRA. Iterative reconstruction of the non-smoothed blank (1 hour) and transmission scans (10 minutes) with the MRP-OSGA method and subsequent calculation of the ACFs produces attenuation corrected emission images without streak artifacts. The study of the quantitative subtraction image of the reconstructed cross section from the liver, using OSEM and the two different approaches for the attenuation correction, is also shown in Figure 6. The main difference between those images is the streak artifact along the patient's arms. This is eliminated in the case of the OSEM reconstruction with the use of iteratively reconstructed transmission scan.

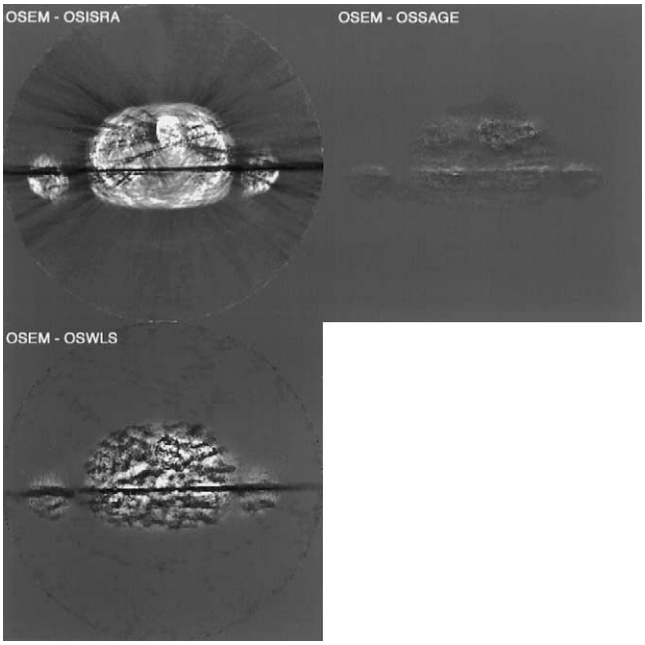

Figure 6. Difference images from the reconstructed cross sections shown in Figure 5. The quantitative subtraction is shown of the OSEM reconstructed image from the image reconstructed with OSISRA (upper left), OSSAGE (upper right), and OSWLS (lower right).

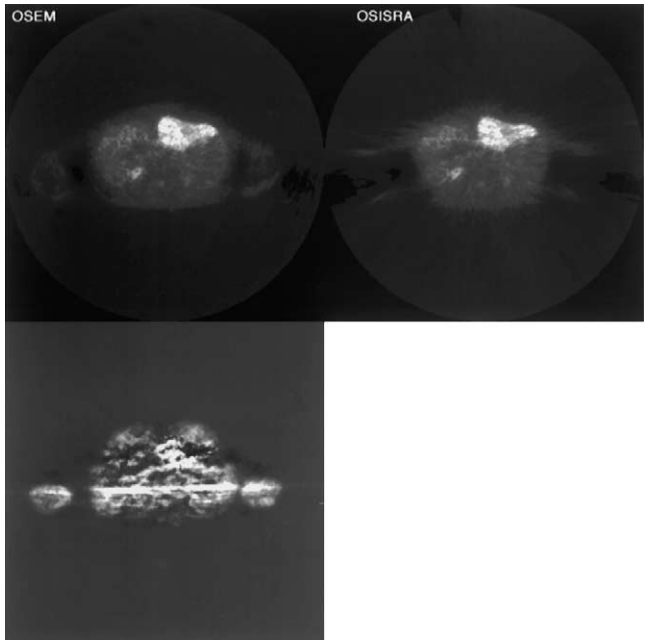

Figure 7. Cross sections from the same liver study shown in Figure 5 (upper row), with OSEM (upper left) and OSISRA (upper right) after attenuation correction using the ACFs calculated after iterative reconstruction of the transmission scans, using the same reconstruction parameters. The quantitative subtraction is shown (lower left) between the OSEM reconstructed cross section shown in Figure 5 and the OSEM reconstructed image shown here.

In summary of the above results, the ordered subsets approach and the approach of the MRP Bayesian regularization of iteratively reconstructed images from clinical PET data sets, either dynamic or static, allow both efficient performance and noise control for the MLEM, ISRA, WLS, and SAGE algorithms. Furthermore, an adequate solution has been presented to the problem of artifacts in the emission images due to suboptimal attenuation correction, with the use of the estimation of the attenuation correction factors from iteratively reconstructed attenuation maps. Optimal selection of the reconstruction parameters for each acquisition protocol can be performed with the methodology presented here. In addition, the implementation framework (distributed PC workstations and Web-based interface) can be easily applied and used by nuclear medicine physicians and scientists in their daily clinical routine. The critical step of the transition of iterative image reconstruction for emission tomography from the level of research investigations to applied clinical use has been achieved.

Conclusions

IIR methods for emission tomography have been briefly discussed, with emphasis on the EM, WLS, ISRA, and SAGE algorithms, with the use of MRP to control noise in the reconstructed images. Ordered-subsets acceleration has been applied to all these methods significantly accelerating their convergence rate. A quantitative study of the quality of the reconstructed images, revealed that the MRP-OSEM method provides the best results on the data typically acquired at the Medical PET Group of the German Cancer Research Center at four to eight iterations and four subsets, using values around 0.2–0.4 for the MRP coefficient.

Application of the median root prior regularization and ordered subsets acceleration has been extended to the case of iterative reconstruction of the transmission images with the gradient algorithm. The use of the MRP- OSGA technique allows a more accurate calculation of the attenuation correction coefficients than the conventional method using the smoothed ratio of the blank and transmission scans. Its application leads to improved quality of the iteratively reconstructed emission images by removing streak artifacts in the reconstructed emission images along high attenuation paths.

In order to bring the above results to the daily routine of a typical PET center, an efficient implementation of the IIR methods presented has been described, using fast-networked PC workstations and a Web-based interface. This work showed that IIR for clinical PET, even for multi-frame dynamic studies, does not require dedicated high-performance computing systems. Efficient reconstruction can be achieved with better management of the existing infrastructure (usually in PCs) in a PET center, using distributed processing principles. A main advantage of the approach proposed here is the physical separation of the reconstruction software from its interface. The user is able to input the desired reconstruction parameters for a particular investigation using a Web-based form, accessible even from outside the center.

One frame (with 63 cross-section slices) from a typical PET scan with the tomograph used can be reconstructed in less than 10 minutes (depending on the parameters and methods used), whereas, a complete dynamic study of 23 such frames can be reconstructed in about three to four hours[44] immediately following the completion of the data acquisition. The quasi-parallel implementation scheme allows the simultaneous reconstruction of several such investigations on the available workstations operating on the network. The approach presented here opens the way for the efficient clinical implementation and practical use of modern iterative image reconstruction schemes in the everyday PET clinical routine.

This work has been partly supported by a Marie Curie Fellowship (HPMF-CT-1999-000274) from the European Commission; project TIC99-1085-CO2 from the Spanish Government; III PRICIT from Comunidad de Madrid; and a scientific cooperation project between Spain and Greece, sponsored by the Spanish Ministry of Foreign Affairs and the Greek Ministry of Development. T. Thireou acknowledges support by the State Fellowships Foundation (IKY, 32nd Fellowships Programme for Graduate Studies) of Greece for doctoral studies in the field of Biomedical Technology

References

1. Barrett, H.H.; Wilson, D.W.; Tsui, B.W. Noise properties of the EM algorithm. I. Theory. Phys.Med. Biol. 39:833–846; 1994.
2. Schiepers, C.; Nuyts, J.; Wu, H.M.; Verma, R.C. PET with 18-F-fluoride: effects of iterative versus filtered backpropagation reconstruction on kinetic modeling. IEEE Trans. Nucl. Sci. 44:1591–1593; 1997.
3. Riddell, C.; Carson, R.E.; Carrasquillo, J.A., et al. Noise reduction in oncology FDG images by iterative reconstruction: a quantitative assessment. J. Nucl. Med. 42: 1316–1323; 2001.
4. Kontaxakis, G.; Strauss, L.G. Maximum likelihood algorithms for image reconstruction in positron emission tomography. In: Limouris, G.S.; Shukla, S.K.; Bender, H.F.; Biersack, H.-J., eds. Radionuclides for oncology - current status and future aspects. Athens, Greece: MEDITERRA Publishers; 1998: 73–106.
5. Strauss, L.G. F-18 deoxyglucose and false-positive results: a major problem in the diagnostics of oncological patients. Eur. J. Nucl. Med. 23: 1409–1415; 1996.
6. Ballesteros Roselló, F.J.; Sánchez Martínez, F.; Reglero Velasco, V. The EM imaging reconstruction method in γ-ray astronomy. Nucl. Instr. Meth. Phys. Res. 145: 469–481; 1998.
7. Miller, M.I.; Butler, C.S. 3D Maximum *a posteriori* estimation for single photon emission tomography on massively parallel computers. IEEE Trans. Med. Imag. 12: 560–565; 1993.
8. Guerrero, T.M; Cherry, S.R.; Dahlbom, M.; Ricci, A.R.; Hoffman, E.J. Fast implementations of 3D PET reconstruction using vector and parallel programming techniques. IEEE Trans. Nucl. Sci. 40: 1082–1086; 1993.
9. Formiconi, A.R.; Passeri, A.; Guelfi, M.R., et al. World Wide Web interface for advanced SPECT reconstruction algorithms implemented on a remote massively parallel computer. Int. J. Med. Inform. 47:125–138; 1997.
10. Johnson, C.A.; Sofer, A. A data-parallel algorithm for tomographic image recontruction. Proc., 7th IEEE Symp. Front. Mass. Parallel Comput. Washington D.C.: IEEE Computer Society Press; 1999: 126 –137.
11. Knoll, P; Gröller, E; Höll, K.; et al. A Jini service to reconstruct tomographic data. IEEE Trans. Med. Imag. 19: 1258–1261; 2000.
12. Shepp, L.A.; Vardi, Y. Maximum likelihood reconstruction in PET. IEEE Trans. Med. Imag. 1:113–122; 1982.
13. Lange, K.; Carson, R. EM reconstruction algorithms for emission and transmission tomography. J. Comp. Ass. Tomogr. 8:302–316; 1984.

14. Anderson, J.M.M.; Mair, B.A.; Rao, M.; Wu, C.-H. Weighted least-squares reconstruction methods for positron emission tomography. IEEE Trans. Med. Imag. 2: 159–165; 1997.
15. Daube-Witherspoon, M.E.; Muehllehner, G. An iterative image reconstruction algorithm suitable for volume ECT. IEEE Trans. Med. Imag. 5: 16–22; 1986.
16. Fessler, J.A.; Hero, A. A space alternating generalized EM algorithm. IEEE Trans. Sig. Proc. 42: 2667–2677; 1994.
17. Hudson, H.M.; Larkin, R.S. Accelerated image reconstruction using ordered subsets of projection data. IEEE Trans. Med. Imag. 13: 601–609; 1994.
18. Mumcuoğlu, E.U.; Leahy, R.; Cherry, S.R. Bayesian reconstruction of PET images: methodology and performance analysis. Phys. Med. Biol. 41:1777–1807; 1996.
19. Green, P. Bayesian reconstructions from emission tomography data using a modified EM algorithm. IEEE Trans. Med. Imag. 9:84–93; 1990.
20. Alenius, S.; Ruotsalainen, U. Bayesian image reconstruction for emission tomography based on median root prior. Eur. J. Nuc. Med. 24: 258–265; 1997.
21. Defrise, M.; Kinahan, P.E.; Townsend, D.W.; et al. Exact and approximate rebinning algorithms for 3D-PET data. IEEE Trans. Med. Imag. 16:145–158; 1997.
22. Liu, X.; Comtat, C.; Michel, C., et. al. Comparison of 3-D reconstruction with 3D-OSEM and with FORE+OSEM for PET. IEEE Trans. Med. Imag. 20: 804–814; 2001.
23. Krzywinski, M.; Sossi, V.; Ruth, T.J. Comparison of FORE, OSEM and SAGE algorithms to 3DRP in 3D PET using phantom and human subject data. IEEE Trans. Nucl. Sci. 46: 1114 –1120; 1999.
24. Richardson, W.H. Bayesian-based iterative method of image restoration. J. Opt. Soc. Am. 62: 55–59; 1972.
25. Lucy, L.B. An iterative technique for the rectification of observed distributions. The Astron. J. 79: 745–754; 1974.
26. Rockmore, A.J.; Macovski, A. A maximum likelihood approach to emission image reconstruction from projections. IEEE Trans. Nucl. Sci. 23:1428–1432; 1976.
27. Dempster, A.P.; Laird, N.M.; Rubin, D.B. Maximum likelihood from incomplete data via the EM algorithm. J. Roy. Stat. Soc. B, 39:1–38, 1977.
28. De Pierro, A.R. On the relation between the ISRA and the EM algorithm for PET. IEEE Trans. Med. Imag. 12: 328–333; 1993.
29. Yavuz, M.; Fessler, J.A. Penalized-likelihood estimators and noise analysis for randoms-precorrected PET transmission scans. IEEE Trans. Med. Imag. 18: 665 -674; 1999.
30. Chinn, G.; Sung-Cheng, H. A general class of preconditioners for statistical iterative reconstruction of emission computed tomography. IEEE Trans. Med. Imag. 16: 1–10; 1997.
31. Kontaxakis, G.; Tzanakos, G. A simulation study of the convergence properties of the EM algorithm for image reconstruction in PET. In: Proceedings 14th IEEE-EMBS Annual International Conference 5:1829–1830; 1992.
32. Veklerov, E.; Llacer J. Feasible images and practical stopping rules for iterative algorithms in emission tomography. IEEE Trans. Med. Imag. 8: 186–193; 1989.
33. Coackley, K.J.; Llacer, J. The use of cross-validation as a stopping rule in emission tomography image reconstruction. Image Phys.1443: 226–233; 1991.
34. Kontaxakis, G.; Tzanakos G. A stopping criterion for the iterative EM-MLE image reconstruction for PET. In: Loew, M.H.; Hanson, K.M., eds. SPIE Proceedings Medical Imaging. Image Proc. 2710: 133–144; 1996.
35. Mumcuoğlu, E.Ü.; Leahy, R.; Cherry, S. Bayesian reconstruction of PET images: methodology and performance analysis. Phys. Med. Biol. 41: 1777–1807; 1996.
36. Lange, K.; Bahn, M.; Little, R. A theoretical study of some maximum likelihood algorithms for emission and transmission tomography. IEEE Trans. Med. Imag. 6:106–114; 1987.
37. Lange, K.; Fessler, J.A. Globally convergent algorithms for maximum a posteriori transmission tomography. IEEE Trans. Imag. Proc. 4: 1430 –1438; 1995.
38. Kamphuis, C.; Beekman, F.J.; Viergever, M.A. Evaluation of OS-EM vs. ML-EM for 1D, 2D and fully 3D SPECT reconstruction. IEEE Trans. Nucl. Sci. 43: 2018–2024; 1996.
39. Byrne, C.L. Accelerating the EMML algorithm and related iterative algorithms by rescaled block-iterative methods. IEEE Trans. Imag. Proc. 7: 100–109; 1998.
40. Soares, E.J.; Byrne, C.L.; Glick, S.J. Noise characterization of block-iterative reconstruction algorithms. I. Theory. IEEE Trans. Med. Imag. 19: 261–270; 2000.
41. Erdogan, H.; Fessler, J.A. Ordered subsets algorithms for transmission tomography. Phys. Med. Biol. 44: 2835–2851; 1999.
42. Alenius, S.; Ruotsalainen, U.; Astola, J. Attenuation correction for PET using count-limited transmission images reconstructed with median root prior. IEEE Trans. Nucl. Sci. 46: 646 –651; 1999.
43. Cox, C.; Schaer, K.; Mobley, C. Fast distributed EM computation for PET image reconstruction using ordered subsets. IEE Colloq. Adv. Electr.Tomogr. (Digest No: 1196/143): 8/1–8/6; 1996.
44. Strauss, L.G.; Kontaxakis, G.; Dimitrakopoulou-Strauss, A. Performance characteristics of iterative image reconstruction techniques for routine use in positron emission tomography. Alasbimn Journal 4: 2001. Available at: http:// www.alasbimn-journal.cl/revistas/13/strauss.html.
45. Kontaxakis, G.; Strauss, L.G.; Tzanakos, G. An efficient implementation of the iterative MLEM image reconstruction algorithm for PET on a Pentium PC platform. J. Comp. Inf. Tech. 7: 153–163; 1999.
46. Kontaxakis, G.; Strauss, L.G.; van Kaick, G. Optimized image reconstruction for emission tomography using ordered subsets, median root prior and a web-based interface. IEEE Trans. Med. Imag. 2:1347–1352; 1998.
47. Hoffman, E.J.; Cutler, P.D.; Digby, W.M.; Mazziotta, J.C. 3-D phantom to simulate cerebral blood flow and metabolic images for PET. IEEE Trans. Nucl. Sci. 37: 616–620, 1990.
48. Toft, P. A very fast implementation of 2D iterative reconstruction algorithms. IEEE Nucl. Sci. Symp. 3: 1742–1746; 1996.
49. Fessler, J.A.; Hero, A. Penalized maximum–likelihood image reconstruction using space-alternating generalized EM algorithms. IEEE Trans. Imag. Proc. 4: 1417–1429, 1995.
50. Seret, A. Median root prior and ordered subsets in Bayesian image reconstruction of single-photon emission tomography. Eur. J. Nucl. Med. 25: 215–219; 1998.
51. Liow, J.-S.; Zho, L. Evaluating performance of reconstruction algorithms for 3-D 15-O water PET using subtraction analysis. IEEE Trans. Med. Imag. 19: 522–531; 2000.
52. Alenius, S.; Ruotsalainen, U. Improving the visual quality of median root prior images in PET and SPECT reconstruction. IEEE Nucl Sci. Symp. 2:15/216 –215/223; 2000.